# Photomodulated Fluorescence of Supramolecular Assemblies of Sulfonatocalixarenes and Tetraphenylethene

**Bang-Ping Jiang, Dong-Sheng Guo, Yan-Cen Liu, Kun-Peng Wang, and Yu Liu***

Department of Chemistry, State Key Laboratory of Elemento-Organic Chemistry, Nankai University, Tianjin 300071, People's Republic of China

**ABSTRACT** Self-assembled fluorescent nanoparticles responding to specific stimuli are highly appealing for applications such as labels, probes, memory devices, and logic gates. However, organic analogues are challenging to prepare, due to unfavorable aggregation-caused quenching. We herein report the preparation of self-assembled fluorescent organic nanoparticles in water by means of calixarene-induced aggregation of a tetraphenylethene derivative (QA-TPE) mediated by *p*-sulfonatocalix[4]arenes. The self-assembled nanoparticles showed interesting photoswitching behaviors, and the fluorescence output of the generated nanoparticles was opposite to that of free QA-TPE both before and after irradiation. Free QA-TPE is nonfluorescent, owing to intramolecular rotations of the phenyl rings. In contrast, the self-assembled nanoparticles that formed upon complexation of QA-TPE with *p*-sulfonatocalix[4]arene exhibited aggregation-induced emission fluorescence ($\lambda_{em}$ = 480 nm, $\Phi$ = 14%), as a result of the inhibition of rotations. Upon UV light irradiation, free QA-TPE was cyclized to the corresponding diphenylphenanthrene, which showed typical fluorescence of a $\pi$-conjugated system ($\lambda_{em}$ = 385 nm, $\Phi$ = 9.3%), whereas the nanoparticles were nonfluorescent upon irradiation due to the aggregation-caused quenching. In effect, this system allows programmed modulation of TPE fluorescence at two different emission wavelengths by means of host–guest complexation and irradiation. Relative to a single-mode stimulus-responsive system, our new developed system of highly integrated modes into a single molecular unit that can exhibit modulation of fluorescence by multiple stimulus is expected to be more adaptable for practical applications and to show enhanced multifunctionality.

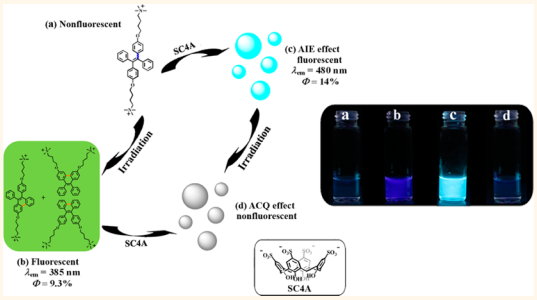


**KEYWORDS:** sulfonatocalixarenes · tetraphenylethene · fluorescent nanoparticle · photoswitching

Fluorescent nanoparticles, and water-soluble species in particular,[1−4] have received increasing attention in recent years due to the fact that they are promising as labels and sensors for cells,[5−7] biomacromolecules,[8,9] small molecules,[10,11] and ions.[12,13] Several strategies have been used to construct fluorescent nanoparticles from organic,[14−19] inorganic,[20] and inorganic−organic hybrid materials.[21−24] Self-assembled fluorescent organic nanoparticles hold great potential because of the variability and flexibility of the starting materials and synthesis methods available.[25,26] However, their utility is restricted by undesired aggregation-caused quenching (ACQ), which is a ubiquitous problem of organic fluorophores.[27,28] Although several approaches, such as encapsulating organic dyes into nanoparticles[29,30] and grafting bulky substituents onto the fluorophores,[31] have been evaluated to diminish ACQ, to some extent, such approaches are helpless to essentially overcome the ACQ effect.

Aggregation-induced emission (AIE), which is essentially the opposite of ACQ, is an extraordinary phenomenon that was first reported by Tang *et al.* in 2001.[32] Molecules that exhibit AIE are nonfluorescent as isolated solubilized species but emit efficiently upon aggregation, due to the restriction of intramolecular rotations.[33] These molecules are therefore attracting more and more interest in the fabrication of fluorescent nanoparticles;[34−38] for example, tetraphenylethene (TPE) behaves as a novel chemo- and bioprobe that shows marked AIE.[35,39−41]

* Address correspondence to yuliu@nankai.edu.cn.

Received for review November 15, 2013 and accepted January 27, 2014.

**Published online January 27, 2014**
**10.1021/nn405923b**

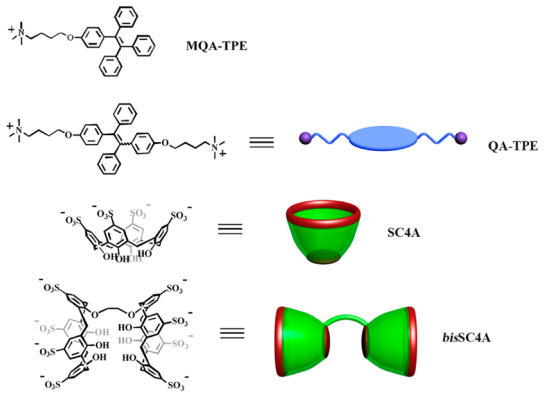


**Chart 1. 4-[4-(*N*,*N*,*N*-Trimethylammonium)butoxy]phenyl-1,2- tetraphenylethene bromide (MQA-TPE), 1,2-bis{4-[4-(*N*,*N*,*N*-trimethylammonium)butoxy]phenyl}-1,2-tetraphenylethene (QA-TPE), *p*-sulfonatocalix[4]arene (SC4A), and bis(*p*-sulfonatocalix[4]arenes) (bisSC4A) (counterions are omitted for clarity).**

Recently, we proposed a novel strategy for the construction of supramolecular assemblies *via* calixarene-induced aggregation (CIA): complexation with *p*-sulfonatocalix[*n*]arenes (SC*n*As, *n* = 4−8) promotes the aggregation of aromatic or amphiphilic molecules by lowering the critical aggregation concentration (CAC), enhancing the aggregate stability, and regulating the degree of order in the aggregates.[42−56] This behavior of calixarenes is opposite that of other commonly studied macrocycles, such as crown ethers, cyclodextrins, and cucurbiturils, which prevent aggregation of guest molecules.[57−59] For example, complexation with SC*n*As promotes the aggregation of quaternary ammonium-modified perylene bisimides,[45] whereas cucurbit[8]uril prevents it.[58]

In this study, combining the advantages of both AIE and CIA, we constructed unique water-soluble fluorescent organic nanoparticles *via* self-assembly of quaternary ammonium-modified TPE (QA-TPE) and SC4As (Chart 1), whereas free QA-TPE is incapable of forming fluorescent nanoparticles, owing to its weak aggregation ability. In addition, in order to isolate specific signals of interest, modulating fluorophores between bright and dark states,[60,61] especially for photoswitching,[62−64] is highly desirable for fluorescent probes,[65] memory devices,[66] logic gates,[67] *etc*. For further practical applications, and also to enhance the multifunctionality of these systems, it is better to combine highly integrated modes into a single molecular unit that can exhibit multistimulus modulation of fluorescence.[68] However, most of these systems employ a fluorescence on−off switching strategy in only single-mode stimulus response. In our work, TPE analogues are photoreactive,[69−71] allowing for photoswitching fluorescence of their assemblies. Therefore, our nanoparticle system exhibited a total of four states, two fluorescent and two nonfluorescent (Scheme 1), and could be modulated by multiple stimulus, revealing a new system of highly integrated fluorescence modes, which is expected to be adaptable for further practical applications.

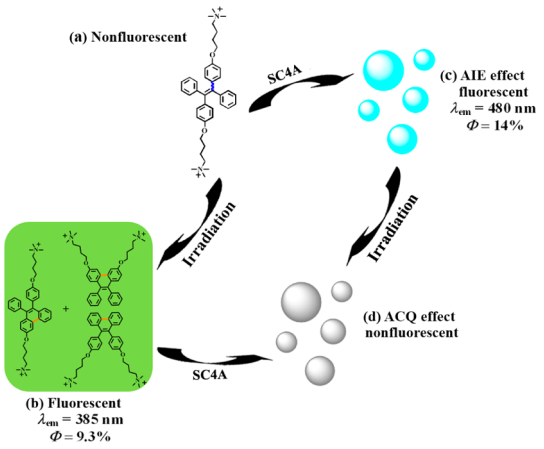


**Scheme 1. Schematic illustration of the fluorescence transitions of QA-TPE induced by host−guest complexation and irradiation: (a) nonfluorescent QA-TPE, (b) fluorescent 1,2-bis{4-[4-(*N*,*N*,*N*-trimethylammonium)butoxy]phenyl}-1,2-diphenylphenanthrene (QA-DPP), (c) fluorescent SC4A+QA-TPE nanoparticles, and (d) nonfluorescent SC4A+QA-DPP nanoparticles.**

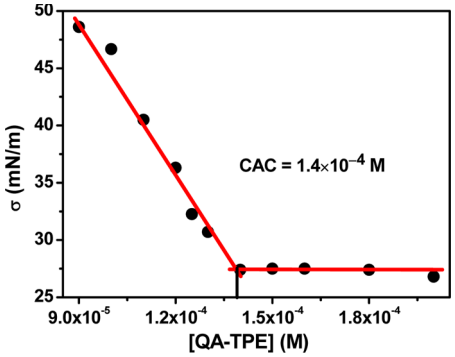


**Figure 1. Dependence of surface tension ($\sigma$) on QA-TPE concentration in water at 25 °C.**

## RESULTS AND DISCUSSION

**CIA of QA-TPE.** SC*n*As are a family of water-soluble calixarene derivatives with three-dimensional, flexible, $\pi$-election-rich cavities and have been widely used in molecular recognition, sensing, and self-assembly applications on account of their intriguing inclusion capabilities.[72] SC*n*As not only form host−guest complexes in conventional 1:1 stoichiometry but also form 1:*n* complexes with certain aromatic or amphiphilic molecules, leading to highly ordered aggregates by means of CIA.[42−56]

Before studying the aggregation of QA-TPE induced by complexation with calixarenes, we first evaluated the aggregation behavior of free QA-TPE. Because QA-TPE is a bolaamphiphile, we examined its aggregation behavior by surface tension measurements (Figure 1). The surface tension of aqueous solutions of QA-TPE decreased linearly as the concentration of QA-TPE was

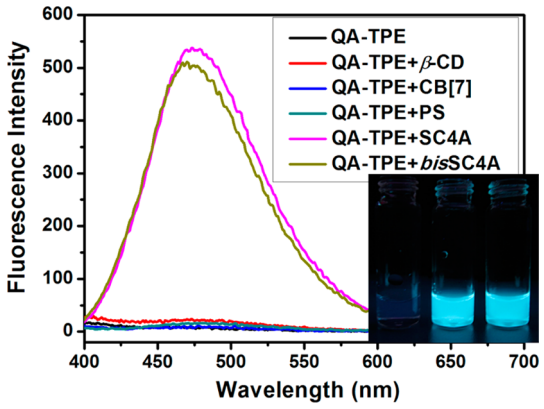


**Figure 2. Fluorescence spectra of QA-TPE ($7.2 \times 10^{-5}$ M) with $\beta$-cyclodextrin ($\beta$-CD, $5.0 \times 10^{-3}$ M), cucurbit[7]uril (CB[7], $1.0 \times 10^{-3}$ M), 4-phenolsulfonic sodium (PS, $2.0 \times 10^{-2}$ M), SC4A ($3.6 \times 10^{-5}$ M), and bisSC4A ($1.8 \times 10^{-5}$ M) in water at 25 °C, $\lambda_{ex}$ = 340 nm. Inset: photographs of QA-TPE (left), QA-TPE+SC4A (center), and QA-TPE+bisSC4A (right) excited by UV light.**

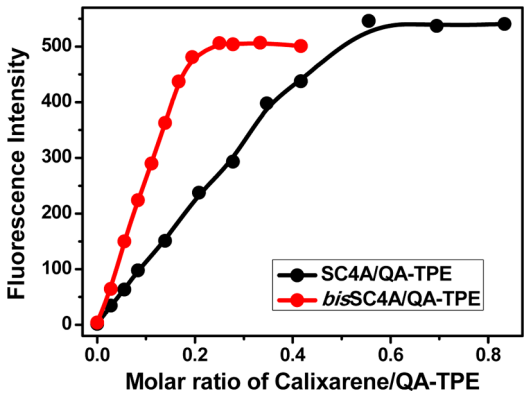


**Figure 3. Change in the fluorescence of QA-TPE at 480 nm upon the gradual addition of SC4A or bisSC4A.**

gradually increased from $9.0 \times 10^{-5}$ to $1.4 \times 10^{-4}$ M, and then remained unchanged at concentrations of $>1.4 \times 10^{-4}$ M, which implies typical aggregation behavior for an amphiphile. The CAC was determined as $1.4 \times 10^{-4}$ M. Dynamic light scattering (DLS) measurement of a QA-TPE solution ($1.5 \times 10^{-4}$ M) showed substantial aggregates with an average hydrodynamic diameter of around 110 nm (Supporting Information Figure S8a), and the aggregates were determined to have spherical morphology by transmission electron microscopy (TEM) (Figure S8b) and atomic force microscopy (AFM) (Figure S8c). However, no appreciable fluorescence of the QA-TPE aggregates was observed (Figure S9). One reasonable explanation is that the free QA-TPE aggregates were not compact enough to restrict intramolecular rotation of the phenyl rings and thus showed no AIE.

When calixarenes were added to the QA-TPE solution, the AIE fluorescence was clearly observed (Figure 2) accompanied by a pronounced complexation-induced decrease in the CAC. In a control experiment, the addition of excess 4-phenolsulfonic sodium (the subunit of SC4A) did not lead to an appreciable change in the fluorescence of QA-TPE, which suggests the crucial role of the preorganized scaffold of the calixarenes in CIA. We also measured the fluorescence of QA-TPE in the presence of $\beta$-cyclodextrin and cucurbit[7]uril, and no AIE fluorescence was observed (Figure 2), indicating that CIA was not induced by these other macrocycles. Two driving factors are indispensable for CIA: (1) the host–guest inclusion interaction offered by the calixarene cavity and (2) the charge interactions between the upper-rim sulfonate groups of calixarene and charged groups of QA-TPE.[42−56] In addition, the AIE fluorescence of QA-TPE could be also observed in water/glycol mixed solvents, which was increased with decreasing water components (Supporting Information Figure S10), similar to previous report about AIE characteristics of TPE.[73]

The binding stoichiometries of SC4A and bisSC4A with QA-TPE were then determined by fluorescence titration (Figure 3 and Figure S11) as well as by Job's method (Figure S12). Upon a stepwise addition of SC4A or bisSC4A to the QA-TPE solution, the fluorescence emission of QA-TPE gradually increased until it reached a plateau when the concentration of SC4A or bisSC4A reached $3.6 \times 10^{-5}$ or $1.8 \times 10^{-5}$ M, respectively (Figure S11). From the inflection points, the host–guest molar ratios could be clearly read as 0.5 for SC4A and 0.25 for bisSC4A, corresponding to 1:2 and 1:4 binding stoichiometries (Figure 3). In the Job plots, the maximum peaks appeared at mole fractions of 0.67 and 0.80, respectively (Figure S12). The obtained host–guest stoichiometries were consistent with the charge matching between the sulfonate groups of the host molecules and the QA groups of the guest molecules. We inferred that the host–guest and charge interactions together drove the CIA. For free QA-TPE, unfavorable electrostatic repulsion between the terminal QA groups offset the favorable $\pi$-stacking and hydrophobic interactions of the TPE spacers; hence, even at high concentrations, only loose aggregates formed without exhibiting AIE. In addition, a mono-quaternary ammonium derivative of TPE (MQA-TPE) (Chart 1) as a comparative compound was employed to investigate aggregation behavior of TPE under the same condition as mentioned before (Figures S13 and S14). The AIE fluorescence was also only observed in the aqueous solution of MQA-TPE upon addition of calixarene, which could not be induced by other macrocycles (Figure S13). In the Job plot, a 1:4 binding stoichiometry was determined as a result of charge matching (Figure S14). These results are consistent with those of QA-TPE and further proved that the multivalent interactions between calixarene and quaternary ammonium-modified TPE derivative together drove the CIA.

We postulate that the CIA observed upon the addition of the calixarenes occurred in two steps

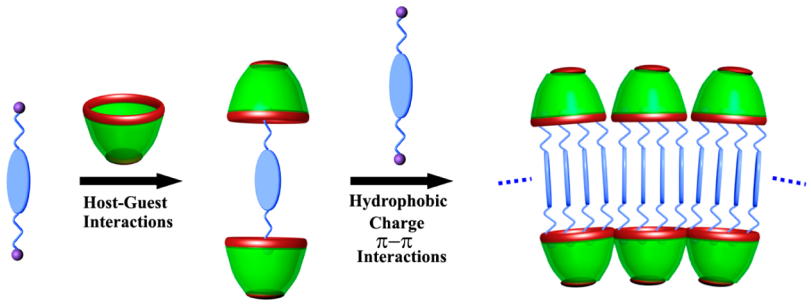


Scheme 2. Schematic illustration of CIA of SC4A and bisSC4A with QA-TPE.

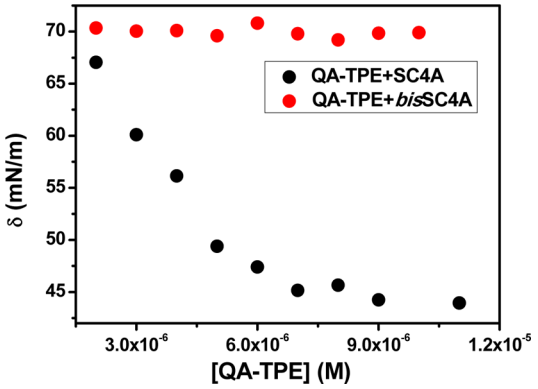


Figure 4. Dependence of the surface tension ($\sigma$) of SC4A+QA-TPE and bisSC4A+QA-TPE solutions on QA-TPE concentration ($2.0 \times 10^{-6}$ to $1.1 \times 10^{-5}$ M) with SC4A or bisSC4A at a 1:1 charge stoichiometry in water at 25 °C.

(Scheme 2). First, the host and guest molecules instantaneously formed a complex in which the two QA groups of the guest were encapsulated by the cavities of two host molecules, affording a 2:1 capsule-like complex driven by the host–guest interaction. Subsequently, additional QA-TPE guest molecules were readily integrated into the 2:1 complexes, which resulted in the formation of compact aggregates with a much lower CAC, due to the fact that the intrinsic electrostatic repulsion between the QA groups was replaced by electrostatic attraction between the QA groups and the sulfonate groups of the host molecules. The resulting aggregates, exhibiting the desired AIE fluorescence, were simultaneously stabilized by noncovalent interactions cooperatively, including host–guest, electrostatic, $\pi$-stacking, and hydrophobic interactions.

To gain more insight into the process of assembly of SC4A and bisSC4A with QA-TPE, we investigated the concentration-dependent surface tension of SC4A+QA-TPE and bisSC4A+QA-TPE solutions (Figure 4). For the SC4A+QA-TPE solution, the surface tension decreased dramatically with increasing concentration until a plateau was reached at $7.0 \times 10^{-6}$ M, implying amphiphilic aggregation with a 1/20 CAC value of free QA-TPE. By contrast, the surface tension of the bisSC4A+QA-TPE solution showed no concentration dependence, indicating non-amphiphilic aggregation.

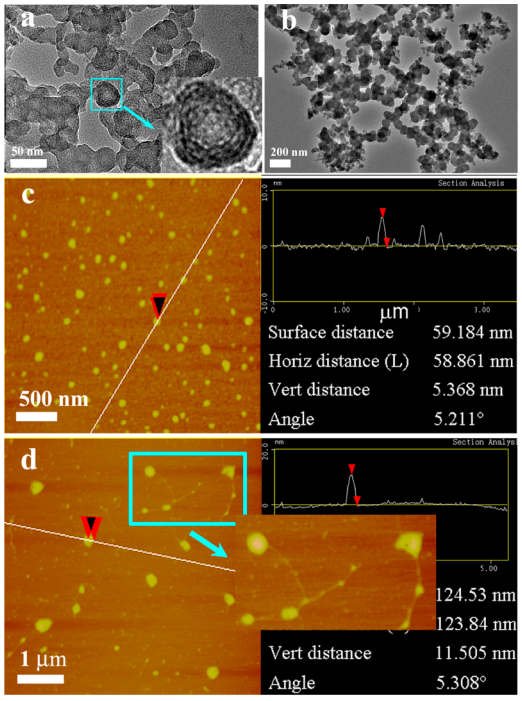


Figure 5. TEM and AFM images: (a,c) SC4A+QA-TPE (QA-TPE, $1.0 \times 10^{-5}$ M; SC4A, $5.0 \times 10^{-6}$ M) and (b,d) bisSC4A+QA-TPE (QA-TPE, $1.0 \times 10^{-5}$ M; bisSC4A, $2.5 \times 10^{-6}$ M).

**Fabricating Fluorescent Nanoparticles by Complexation of Calixarenes with QA-TPE.** On the basis of the results of fluorescence titration and Job plots, we used host–guest ratios of 1:2 for SC4A+QA-TPE and 1:4 for bisSC4A+QA-TPE to fabricate the corresponding fluorescent nanoparticles. The sizes and morphologies of the self-assembled SC4A+QA-TPE and bisSC4A+QA-TPE nanoparticles were determined by DLS, TEM, and AFM, respectively (Supporting Information Figure S15 and Figure 5). In a control experiment, we found that QA-TPE showed no appreciable scattering intensity at $1.0 \times 10^{-5}$ M (Figure S15a), implying that no large aggregates formed. Upon complexation with SC4A or bisSC4A, aggregates with average hydrodynamic diameters of about 60 nm for SC4A+QA-TPE and about 120 nm for bisSC4A+QA-TPE formed (Figure S15b,c). Meanwhile, the DLS measurement was also employed to investigate the aggregation of the SC4A+MQA-TPE complex (Figure S19), showing no appreciable scattering

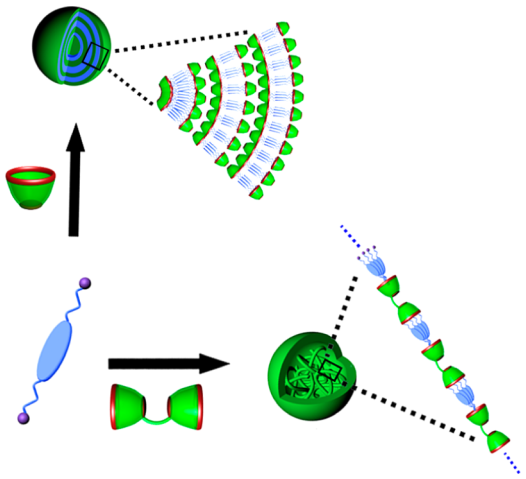

**Scheme 3. Models for assembly of QA-TPE in the presence of SC4A and bisSC4A.**

intensity, which was substantially different from the SC4A+QA-TPE complex. Under the same concentration of TPE, the complexation of SC4A with MQA-TPE can generate the AIE fluorescence (Figure S13) but cannot lead to the formation of large-size aggregates (Figure S19). Compared to QA-TPE, MQA-TPE is one binding site less, and therefore, the host−guest and charge interactions between SC4A and MQA-TPE are not robust enough to drive the formation of large-size aggregates, but probably oligomers were formed. TEM indicated that both the SC4A+QA-TPE and bisSC4A+QA-TPE nanoparticles were spherical, with average diameters of about 30 and 90 nm, respectively (Figure 5a,b). Moreover, the SC4A+QA-TPE nanoparticles showed multilamellar stacks. AFM measurements gave similar results (Figure 5c,d). It should be noted that, in the AFM image of the bisSC4A+QA-TPE nanoparticles, regular linear arrays extending away from the spherical nanoparticles were also observed (Figure 5d). In an effort to gain a deeper understanding of assembly behaviors of calixarenes and QA-TPE, the DLS experiments with different host−guest ratios were performed by maintaining the concentration of QA-TPE ($1.0 \times 10^{-5}$ M) (Figures S16 and S17). The results suggest that, after large-size aggregates have formed, the further increase of the host−guest ratios with a constant concentration of QA-TPE cannot result in change of sizes of the SC4A+QA-TPE and bisSC4A+QA-TPE assemblies.

Taken together, our results suggest the assembly models depicted in Scheme 3. The SC4A+QA-TPE nanoparticles exhibited typical amphiphilic characteristics and a bilayer structure that curved to generate multilamellar spheres. In contrast, the bisSC4A+QA-TPE nanoparticles consisted of linear arrays formed as a result of the two cavities of bisSC4A, and the linear arrays rolled into a random coil stabilized by $\pi$-stacking interactions among the TPE and calixarene units. Confocal fluorescence images showed that both the

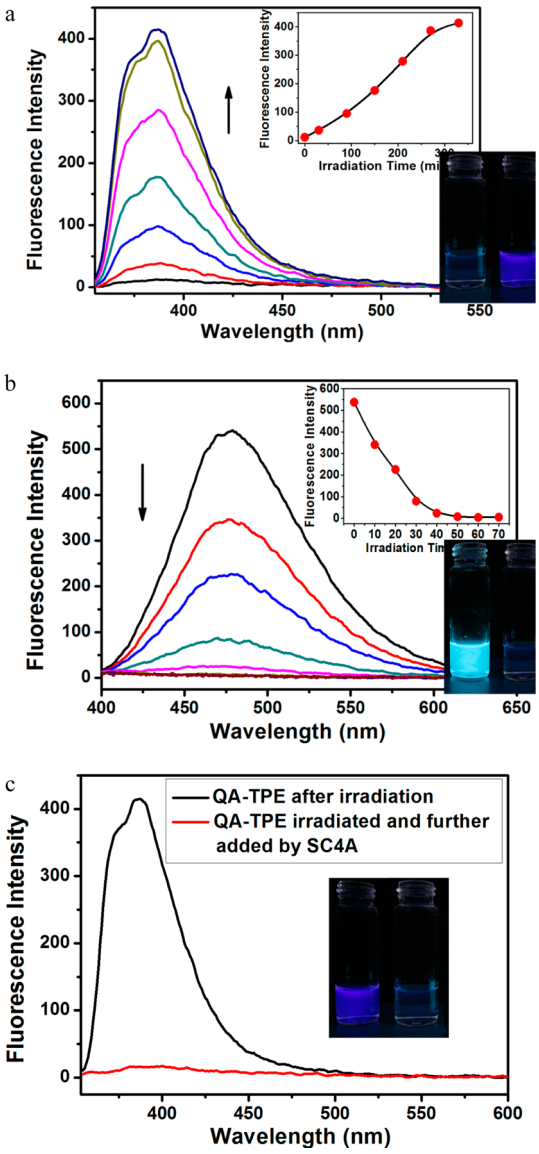


**Figure 6. Fluorescence spectra of (a) free QA-TPE and (b) SC4A+QA-TPE nanoparticles at different irradiation times. Insets: photographs of fluorescence before (left) and after (right) irradiation. (c) Fluorescence spectra of free QA-TPE after irradiation for 310 min and subsequent addition of SC4A. Inset: fluorescence photographs of free QA-TPE after irradiation for 310 min before (left) and after (right) addition of SC4A. [QA-TPE] = $7.2 \times 10^{-5}$ M, [SC4A] = $3.6 \times 10^{-5}$ M, and $\lambda_{ex}$ = 340 nm.**

SC4A+QA-TPE and bisSC4A+QA-TPE nanoparticles exhibited robust blue fluorescence (Figure S18b,c). No such fluorescence was observed with free QA-TPE (or aggregates of QA-TPE above its CAC) (Figure S18a); this result is in good agreement with the results of the above-described fluorescence experiments.

**Fluorescence Modulation by Irradiation.** TPE derivatives are photoreactive, undergoing cyclization to diphenylphenanthrene (DPP) derivatives upon irradiation.[69−71] Given that TPE exhibits AIE and that DPP exhibits ACQ,[70] we decided to examine the fluorescence responses of free QA-TPE and the self-assembled

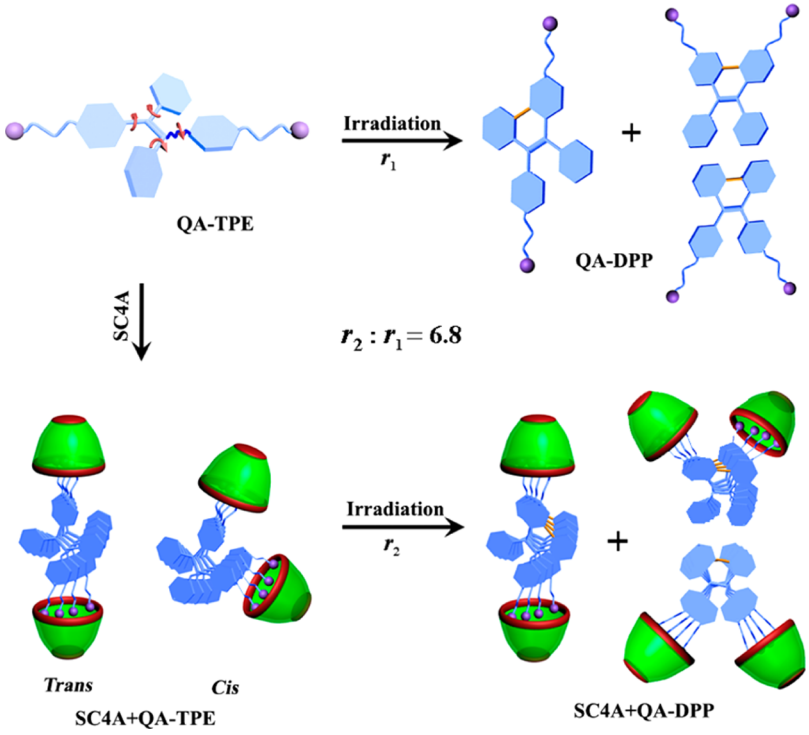


**Scheme 4. Schematic illustration of the photocyclizations of free QA-TPE and the SC4A+QA-TPE nanoparticles.**

nanoparticles to a photostimulus. The SC4A+QA-TPE nanoparticles were employed because SC4A is more readily available than bisSC4A. UV light irradiation of free QA-TPE switched it from nonfluorescent to fluorescent ($\lambda_{em}$ = 385 nm, $\Phi$ = 9.3%; Figure 6a), and the fluorescence could be quenched by adding SC4A at a 1:1 charge stoichiometry (Figure 6c). For the SC4A+QA-TPE nanoparticles, the fluorescence change upon irradiation differed from that of free QA-TPE (Figure 6b), switching from fluorescent ($\lambda_{em}$ = 480 nm, $\Phi$ = 14%) to nonfluorescent.

The mechanisms of the fluorescence changes of free QA-TPE and the SC4A+QA-TPE nanoparticles upon irradiation were investigated by mass spectrometry (MS) and $^1$H NMR measurements (Supporting Information Figures S20−S22). A main peak at 296.4 (Figures S20a and S21a), assigned to $[(QA\text{-}TPE\text{-}2Br)/2]^+$, was observed before irradiation but disappeared almost completely upon irradiation; meanwhile, a new main peak at 295.4 (Figures S20b and S21b), assigned to $[(QA\text{-}TPE\text{-}2Br\text{-}2H)/2]^+$, was observed. Moreover, in the time-dependent $^1$H NMR spectra of QA-TPE (Figure S22), the peaks assigned to the aromatic protons of QA-TPE ($\delta$ = 6.51−7.12 ppm) were passivated, and new signals at $\delta$ = 7.24, 7.37, 7.56, 8.12, and 8.68 ppm emerged after 180 min irradiation (Figure S22a). The signal assigned to $OCH_2$ group ($\delta$ = 3.84 ppm) changed to two singlets with $\delta$ = 3.82 and 4.09 ppm (Figure S22b). This evidence obtained in the MS and $^1$H NMR spectroscopic data clearly confirmed the photoinduced cyclization of QA-TPE to QA-DPP,[70,71] which should have three possible structures due to *cis*/*trans* isomerization of QA-TPE:[74−76] one results from the *trans* isomer; the other two originate from the *cis* isomer (Scheme 4). QA-TPE was nonfluorescent due to unhindered low-frequency intramolecular rotations of the phenyl groups, whereas complexation with calixarene induced the aggregation of QA-TPE, which then triggered the AIE fluorescence by restricting intramolecular rotation of the TPE unit. The photoreaction product QA-DPP showed the typical fluorescence of a $\pi$-conjugated system because the formation of a C−C bond between the neighboring phenyl rings restricted intramolecular rotation. Calixarene also induced the aggregation of QA-DPP, but the fluorescence was quenched by means of ACQ that is generally observed in condensed phase, where the aggregates of the fluorophore are prone to decay through nonradiative pathways rather than luminescent ones.[15] In addition, we also performed irradiation of free MQA-TPE and the SC4A+MQA-TPE complex, which was investigated by fluorescence and MS measurements (Figures S24 and S25), giving similar results to those of free QA-TPE and the SC4A+QA-TPE nanoparticles.

With all these results in hand, we concluded that the programmed modulation of TPE fluorescence with diverse emissions by means of host−guest complexation and irradiation occurred as schematically illustrated in Scheme 1: nonfluorescent QA-TPE turns to be fluorescent QA-DPP, while AIE fluorescent SC4A+QA-TPE nanoparticles turn to be ACQ nonfluorescent SC4A+QA-DPP nanoparticles. Remarkably, the oxidative

photocyclization rate of QA-TPE was markedly accelerated by complexation with SC4A (Figure 6). The photoreaction of SC4A+QA-TPE ($r_2$) was 6.8 times as fast as that of free QA-TPE ($r_1$). One reasonable explanation is that the complexed QA-TPE existed in a compact aggregate, and the intramolecular rotations of the phenyl groups in the TPE unit were effectively restricted by $\pi\cdots\pi$ stacking of the neighboring TPE units, which favored photocyclization of QA-TPE to QA-DPP (Scheme 4). Moreover, oxidative photocyclization rate of aggregates of QA-TPE above its CAC was also studied (Figure S23); however, no acceleration of photoreaction was observed.

## CONCLUSIONS

In summary, we fabricated two types of self-assembled fluorescent organic nanoparticles that exhibited CIA and AIE in aqueous media. When QA-TPE complexed with SC4A and bisSC4A, not only did the CAC decrease markedly but also the $\pi$-aggregation of TPE became more compact. Consequently, the SC4A+QA-TPE and bisSC4A+QA-TPE nanoparticles exhibited the desired AIE fluorescence, which cannot be achieved with free QA-TPE. Photoswitching the fluorescence of free QA-TPE and the self-assembled nanoparticles was also achieved, benefitting from the photoreactivity of TPE. Thus, we were able to achieve a system of nanoparticles with diverse fluorescence modes by means of host−guest complexation and irradiation. Our results can be expected to pave the way for the construction of organic nanoparticle systems with fluorescence that can be modulated by multiple stimuli. Such systems are expected to find practical applications as fluorescent probes, memory devices, and logic gates, among others.

## EXPERIMENTAL SECTION

**Materials.** All chemicals used are reagent grade unless noted. *p*-Sulfonatocalix[4]arene (SC4A)[77] and bis(*p*-sulfonatocalix[4]arenes) (bisSC4A)[78] were synthesized and purified according to previously reported procedures. Trimethylamine was purchased from commercial resources and used without further purification. 4-(4-Bromobutoxy)-phenyl-1,2-tetraphenylethene[79] and 1,2-bis[4-(4-bromobutoxy)phenyl]-1,2-tetraphenylethene[73] were synthesized according to the procedure in the literature.

**Synthesis of 4-[4-(*N*,*N*,*N*-Trimethylammonium)butoxy]phenyl-1,2-tetraphenylethene bromide (MQA-TPE) (Figure S1).** 4-(4-Bromobutoxy)-phenyl-1,2-tetraphenylethene (1450 mg, 3 mmol) was dissolved in a 100 mL flask with a magnetic stir bar and THF (50 mL). After the mixture was placed in an ice bath, an excess amount of trimethylamine gas was introduced. The mixture solution was allowed to warm to room temperature. After being stirred for 1 day, the solvent was removed at reduced pressure. After being dried overnight in vacuum at 45 °C, MQA-TPE was obtained as pale yellow powder (743 mg) in a yield of 48%. $^1$H NMR (400 MHz, $CDCl_3$, $\delta$): 7.09−6.97 (m, 15H), 6.90 (d, 2H), 6.60 (d, 2H), 3.91 (t, 2H), 3.72 (t, 2H), 3.43 (s, 9H), 1.93 (br, 2H), 1.83 (br, 2H). $^{13}$C NMR (100 MHz, $CDCl_3$, $\delta$): 157.04, 143.93, 143.89, 143.83, 140.32, 140.22, 136.44, 132.57, 131.30, 131.28, 127.74, 127.62, 127.60, 126.38, 126.29, 126.27, 113.56, 66.53, 66.34, 53.38, 25.96, 20.03. ESI-MS: 462.3 $(M - Br)^+$. Anal. Calcd for $C_{33}H_{36}BrNO$: C, 73.05; H, 6.69; N, 2.58. Found: C, 73.02; H, 6.72; N, 2.49.

**Synthesis of 1,2-Bis{4-[4-(*N*,*N*,*N*-trimethylammonium)butoxy]phenyl}-1,2- tetraphenylethene dibromide (QA-TPE) (Figure S1).** 1,2-Bis[4-(4-bromobutoxy)-phenyl]-1,2-tetraphenylethene (1896 mg, 3 mmol) was dissolved in a 100 mL flask with a magnetic stir bar and THF (50 mL). After the mixture was placed in an ice bath, an excess amount of trimethylamine gas was introduced. The mixture solution was allowed to warm to room temperature. After being stirred for 1 day, 10 mL of water was added, and then the mixture was continuously stirred for 1 day. The solvent was removed at reduced pressure, and the residue was washed with THF three times. After being dried overnight in vacuum at 45 °C, QA-TPE was obtained as pale yellow powder (1147 mg) in a yield of 51%. $^1$H NMR (400 MHz, $D_2O$, $\delta$): 6.86−6.69 (m, 14H), 6.30 (br, 4H), 3.46 (d, 4H), 3.12 (br, 4H), 2.91 (d, 18H), 1.49 (br, 8H). $^{13}$C NMR (100 MHz, $D_2O$, $\delta$): 156.91, 139.81, 132.30, 131.07, 127.79, 113.99, 67.18, 66.00, 53.06, 25.62, 19.56. ESI-MS: 296.4 $((M - 2Br)/2)^+$. Anal. Calcd for $C_{40}H_{52}Br_2N_2O_2$: C, 63.83; H, 6.96; N, 3.72. Found: C, 63.80; H, 7.01; N, 3.67.

**Measurements.** NMR spectra were recorded on a Bruker AV400 spectrometer. Mass spectra were performed on an LCQ-Advantage MS. Elemental analysis was performed on a Perkin-Elmer 2400C instrument. The surface tension in water was measured by using a QBZY full-automatic surface tensiometer with the method of platinum plate at 25 °C. Steady-state fluorescence spectra were recorded on a Varian Cary Eclipse equipped with a Varian Cary single cell peltier accessory to maintain the temperature.

**Transmission Electron Microscopic (TEM) Measurements.** TEM images were recorded using a Tecnai 20 high-resolution transmission electron microscope operating at an accelerating voltage of 200 keV. The sample of QA-TPE ($1.0 \times 10^{-5}$ M), QA-TPE ($1.5 \times 10^{-4}$ M), SC4A+QA-TPE (QA-TPE, $1.0 \times 10^{-5}$ M; SC4A, $5.0 \times 10^{-6}$ M), and bisSC4A+QA-TPE (QA-TPE, $1.0 \times 10^{-5}$ M; bisSC4A, $2.5 \times 10^{-6}$ M) were prepared by dropping the solution onto a copper grid and then drying in air.

**Atomic Force Microscopic (AFM) Measurements.** The AFM measurements were performed by using an AFM (Veeco Company, Multimode, Nano IIIa) in tapping mode at room temperature. Sample solutions of QA-TPE ($1.5 \times 10^{-4}$ M), SC4A+QA-TPE (QA-TPE, $1.0 \times 10^{-5}$ M; SC4A, $5.0 \times 10^{-6}$ M), and bisSC4A+QA-TPE (QA-TPE, $1.0 \times 10^{-5}$ M; bisSC4A, $2.5 \times 10^{-6}$ M) were dropped onto newly clipped mica and then dried in air.

**Dynamic Light Scattering (DLS) Measurements.** DLS was performed on a laser light scattering spectrometer (BI-200SM) equipped with a digital correlator (BI-9000AT) at 532 nm. All sample solutions for DLS measurements, including MQA-TPE ($1.0 \times 10^{-5}$ M), QA-TPE ($1.0 \times 10^{-5}$ M), QA-TPE ($1.5 \times 10^{-4}$ M), SC4A+MQA-TPE (MQA-TPE, $1.0 \times 10^{-5}$ M; SC4A, $2.5 \times 10^{-6}$ M), SC4A+QA-TPE (QA-TPE, $1.0 \times 10^{-5}$ M; SC4A, $5.0 \times 10^{-6}$ M), and bisSC4A+QA-TPE (QA-TPE, $1.0 \times 10^{-5}$ M; bisSC4A, $2.5 \times 10^{-6}$ M), *etc.*, were prepared by filtering solution through a 450 nm Millipore filter into a clean scintillation vial.

**Confocal Fluorescence Measurements.** The confocal fluorescence images were recorded on a laser confocal microscope (OLYMPUS FV1000S-IX81). Sample solutions of QA-TPE ($1.5 \times 10^{-4}$ M), SC4A+QA-TPE (QA-TPE, $7.2 \times 10^{-5}$ M; SC4A, $3.6 \times 10^{-5}$ M), and bisSC4A+QA-TPE (QA-TPE, $7.2 \times 10^{-5}$ M; bisSC4A, $1.8 \times 10^{-5}$ M) were dropped onto newly clipped mica and immediately used for measurements.

**Irradiation.** The solutions of free MQA-TPE ($7.2 \times 10^{-5}$ M), free QA-TPE ($7.2 \times 10^{-5}$ M), the SC4A+MQA-TPE complex (MQA-TPE, $7.2 \times 10^{-5}$ M; SC4A, $1.8 \times 10^{-5}$ M), and the SC4A+QA-TPE nanoparticle (QA-TPE, $7.2 \times 10^{-5}$ M; SC4A, $3.6 \times 10^{-5}$ M) were placed in a quartz bottle and further irradiated by using a 500 W medium-pressure mercury lamp (CEL-M500) after inletting $N_2$ for 10 min at room temperature.

**Quantum Yield Measurements.** The absolute quantum yields were measured, referring to the procedure in the literature.[80]

They were recorded on an Edinburgh Analytical Instruments FLS920 with an inner diameter of 150 mm integrating sphere coated inside with $BaSO_4$ and calculated by using following equation:

$$\Phi = \frac{f}{\alpha} = \frac{\int L_{emission}}{\int E_{solvent} - \int E_{sample}}$$

where $f$ is the photons emitted by the sample; $\alpha$ is the photons absorbed by the sample; $\Phi$ is the absolute quantum yield; $L_{emission}$ is the luminescence emission spectrum of the sample, collected using the sphere; $E_{sample}$ is the spectrum of the light used to excite the sample, collected using the sphere; and $E_{solvent}$ is the spectrum of the light used for excitation with only the solvent in the sphere, collected using the sphere. Sample solutions of free QA-TPE ($7.2 \times 10^{-5}$ M) after irradiation for 310 min and SC4A+QA-TPE (QA-TPE, $7.2 \times 10^{-5}$ M; SC4A, $3.6 \times 10^{-5}$ M) were used to measure the absolute quantum yields in water at 25 °C, $\lambda_{ex}$ = 340 nm.

**Mass Spectra Measurements for Photoreaction.** The mass spectra measurements were performed after 270, 310, 140, and 45 min irradiation for free MQA-TPE, free QA-TPE, the SC4A+MQA-TPE complex, and the SC4A+QA-TPE assembly, respectively.

*Conflict of Interest:* The authors declare no competing financial interest.

*Acknowledgment.* This work was supported by 973 Program (Grant 2011CB932502) and National Natural Science Foundation of China (Grants 91227107 and 21172119), which are gratefully acknowledged.

*Supporting Information Available:* NMR, ESI-MS spectra of MQA-TPE, QA-TPE, and other data as described in the text. This material is available free of charge *via* the Internet at http://pubs.acs.org.

## REFERENCES AND NOTES


1. Gill, R.; Zayats, M.; Willner, I. Semiconductor Quantum Dots for Bioanalysis. *Angew. Chem., Int. Ed.* **2008**, *47*, 7602–7625.
2. Medintz, I. L.; Uyeda, H. T.; Goldman, E. R.; Mattoussi, H. Quantum Dot Bioconjugates for Imaging, Labelling and Sensing. *Nat. Mater.* **2005**, *4*, 435–446.
3. Tian, Z.; Li, A. D. Q. Photoswitching-Enabled Novel Optical Imaging: Innovative Solutions for Real-World Challenges in Fluorescence Detections. *Acc. Chem. Res.* **2013**, *46*, 269–279.
4. Gorris, H. H.; Wolfbeis, O. S. Photon-Upconverting Nanoparticles for Optical Encoding and Multiplexing of Cells, Biomolecules, and Microspheres. *Angew. Chem., Int. Ed.* **2013**, *52*, 3584–3600.
5. Zhu, L.; Wu, W.; Zhu, M.-Q.; Han, J. J.; Hurst, J. K.; Li, A. D. Q. Reversibly Photoswitchable Dual-Color Fluorescent Nanoparticles as New Tools for Live-Cell Imaging. *J. Am. Chem. Soc.* **2007**, *129*, 3524–3526.
6. Dennis, A. M.; Rhee, W. J.; Sotto, D.; Dublin, S. N.; Bao, G. Quantum Dot-Fluorescent Protein FRET Probes for Sensing Intracellular pH. *ACS Nano* **2012**, *6*, 2917–2924.
7. Wu, C.; Bull, B.; Szymanski, C.; Christensen, K.; McNeill, J. Multicolor Conjugated Polymer Dots for Biological Fluorescence Imaging. *ACS Nano* **2008**, *2*, 2415–2423.
8. Petkau, K.; Kaeser, A.; Fischer, I.; Brunsveld, L.; Schenning, A. P. H. J. Pre- and Postfunctionalized Self-Assembled $\pi$-Conjugated Fluorescent Organic Nanoparticles for Dual Targeting. *J. Am. Chem. Soc.* **2011**, *133*, 17063–17071.
9. Feng, X.; Liu, L.; Wang, S.; Zhu, D. Water-Soluble Fluorescent Conjugated Polymers and Their Interactions with Biomacromolecules for Sensitive Biosensors. *Chem. Soc. Rev.* **2010**, *39*, 2411–2419.
10. Zhang, K.; Zhou, H.; Mei, Q.; Wang, S.; Guan, G.; Liu, R.; Zhang, J.; Zhang, Z. Instant Visual Detection of Trinitrotoluene Particulates on Various Surfaces by Ratiometric Fluorescence of Dual-Emission Quantum Dots Hybrid. *J. Am. Chem. Soc.* **2011**, *133*, 8424–8427.
11. Fercher, A.; Borisov, S. M.; Zhdanov, A. V.; Klimant, I.; Papkovsky, D. B. Intracellular $O_2$ Sensing Probe Based on Cell-Penetrating Phosphorescent Nanoparticles. *ACS Nano* **2011**, *5*, 5499–5508.
12. Chan, Y.-H.; Wu, C.; Ye, F.; Jin, Y.; Smith, P. B.; Chiu, D. T. Development of Ultrabright Semiconducting Polymer Dots for Ratiometric pH Sensing. *Anal. Chem.* **2011**, *83*, 1448–1455.
13. Chen, W.; Tu, X.; Guo, X. Fluorescent Gold Nanoparticles-Based Fluorescence Sensor for $Cu^{2+}$ Ions. *Chem. Commun.* **2009**, 1736–1738.
14. Pecher, J.; Mecking, S. Nanoparticles of Conjugated Polymers. *Chem. Rev.* **2010**, *110*, 6260–6279.
15. Thomas, S. W.; Joly, G. D.; Swager, T. M. Chemical Sensors Based on Amplifying Fluorescent Conjugated Polymers. *Chem. Rev.* **2007**, *107*, 1339–1386.
16. Jatsch, A.; Schillinger, E.-K.; Schmid, S.; Böauerle, P. Biomolecule Assisted Self-Assembly of $\pi$-Conjugated Oligomers. *J. Mater. Chem.* **2010**, *20*, 3563–3578.
17. Landfester, K. Miniemulsion Polymerization and the Structure of Polymer and Hybrid Nanoparticles. *Angew. Chem., Int. Ed.* **2009**, *48*, 4488–4507.
18. Jaskiewicz, K.; Larsen, A.; Lieberwirth, I.; Koynov, K.; Meier, W.; Fytas, G.; Kroeger, A.; Landfester, K. Probing Bioinspired Transport of Nanoparticles into Polymersomes. *Angew. Chem., Int. Ed.* **2012**, *51*, 4613–4617.
19. Zhang, X.; Yu, J.; Rong, Y.; Ye, F.; Chiu, D. T.; Uvdal, K. High-Intensity Near-IR Fluorescence in Semiconducting Polymer Dots Achieved by Cascade FRET Strategy. *Chem. Sci.* **2013**, *4*, 2143–2151.
20. Haase, M.; Schäfer, H. Upconverting Nanoparticles. *Angew. Chem., Int. Ed.* **2011**, *50*, 5808–5829.
21. Morgan, T. T.; Muddana, H. S.; Altinoglu, E. I.; Rouse, S. M.; Tabakivic, T.; Tabouillot, T.; Russin, T. J.; Shanmugavelandy, S. S.; Butler, P. J.; Eklund, P. C.; *et al.* Encapsulation of Organic Molecules in Calcium Phosphate Nanocomposite Particles for Intracellular Imaging and Drug Delivery. *Nano Lett.* **2008**, *8*, 4108–4115.
22. Roming, M.; Lünsdorf, H.; Dittmar, K. E. J.; Feldmann, C. $ZrO(HPO_4)_{1-x}(FMN)_x$: Quick and Easy Synthesis of a Nanoscale Luminescent Biomarker. *Angew. Chem., Int. Ed.* **2010**, *49*, 632–637.
23. Chan, Y.-H.; Ye, F.; Gallina, M. E.; Zhang, X.; Jin, Y.; Wu, I.-C.; Chiu, D. T. Hybrid Semiconducting Polymer Dot-Quantum Dot with Narrow-Band Emission, Near-Infrared Fluorescence, and High Brightness. *J. Am. Chem. Soc.* **2012**, *134*, 7309–7312.
24. Burns, A.; Ow, H.; Wiesner, U. Fluorescent Core−Shell Silica Nanoparticles: Towards "Lab on a Particle" Architectures for Nanobiotechnology. *Chem. Soc. Rev.* **2006**, *35*, 1028–1042.
25. An, B.-K.; Kwon, S.-K.; Jung, S.-D.; Park, S. Y. Enhanced Emission and Its Switching in Fluorescent Organic Nanoparticles. *J. Am. Chem. Soc.* **2002**, *124*, 14410–14415.
26. Jana, A.; Devi, K. S. P.; Maiti, T. K.; Singh, N. D. P. Perylene-3-ylmethanol: Fluorescent Organic Nanoparticles as a Single-Component Photoresponsive Nanocarrier with Real-Time Monitoring of Anticancer Drug Release. *J. Am. Chem. Soc.* **2012**, *134*, 7656–7659.
27. Zhao, Q.; Li, K.; Chen, S.; Qin, A.; Ding, D.; Zhang, S.; Liu, Y.; Liu, B.; Sun, J. Z.; Tang, B. Z. Aggregation-Induced Red-NIR Emission Organic Nanoparticles as Effective and Photostable Fluorescent Probes for Bioimaging. *J. Mater. Chem.* **2012**, *22*, 15128–15135.
28. Qiu, F.; Zhu, Q.; Tong, G.; Zhu, L.; Wang, D.; Yan, D.; Zhu, X. Highly Fluorescent Core−Shell Hybrid Nanoparticles Templated by a Unimolecular Star Conjugated Polymer for a Biological Tool. *Chem. Commun.* **2012**, *48*, 11954–11956.
29. Wu, C.; Chiu, D. T. Highly Fluorescent Semiconducting Polymer Dots for Biology and Medicine. *Angew. Chem., Int. Ed.* **2013**, *52*, 3086–3109.
30. Jin, Y.; Ye, F.; Zeigler, M.; Wu, C.; Chiu, D. T. Near-Infrared Fluorescent Dye-Doped Semiconducting-Polymer Dots. *ACS Nano* **2011**, *5*, 1468–1475.
31. Kaeser, A.; Fischer, I.; Abbel, R.; Besenius, P.; Dasgupta, D.; Gillisen, M. A. J.; Portale, G.; Stevens, A. L.; Herz, L. M.;

Schenning, A. P. H. J. Side Chains Control Dynamics and Self-Sorting in Fluorescent Organic Nanoparticles. *ACS Nano* **2013**, *7*, 408–416.
32. Luo, J.; Xie, Z.; Lam, J.; Cheng, L.; Chen, H.; Qiu, C.; Kwok, H. S.; Zhan, X.; Liu, Y.; Zhu, D.; *et al.* Aggregation-Induced Emission of 1-Methyl-1,2,3,4,5-pentaphenylsilole. *Chem. Commun.* **2001**, 1740–1741.
33. Hong, Y.; Lam, J. W. Y.; Tang, B. Z. Aggregation-Induced Emission: Phenomenon, Mechanism and Applications. *Chem. Commun.* **2009**, 4332–4353.
34. Kumar, M.; George, S. J. Green Fluorescent Organic Nanoparticles by Self-Assembly Induced Enhanced Emission of a Naphthalene Diimide Bolaamphiphile. *Nanoscale* **2011**, *3*, 2130–2133.
35. Chen, S.; Liu, J.; Liu, Y.; Su, H.; Hong, Y.; Jim, C. K. W.; Kwok, R. T. K.; Zhao, N.; Qin, W.; Lam, J. W. Y.; *et al.* An AIE-Active Hemicyanine Fluorogen with Stimuli-Responsive Red/Blue Emission: Extending the pH Sensing range by "Switch + Knob" Effect. *Chem. Sci.* **2012**, *3*, 1804–1809.
36. Patra, A.; Scherf, U. Fluorescent Microporous Organic Polymers: Potential Testbed for Optical Applications. *Chem.—Eur. J.* **2012**, *18*, 10074–10080.
37. An, B.-K.; Kwon, S.-K.; Park, S. Y. Photopatterned Arrays of Fluorescent Organic Nanoparticles. *Angew. Chem., Int. Ed.* **2007**, *46*, 1978–1982.
38. Wang, M.; Zhang, G.; Zhang, D.; Zhu, D.; Tang, B. Z. Fluorescent Bio/chemosensors Based on Silole and Tetraphenylethene Luminogens with Aggregation-Induced Emission Feature. *J. Mater. Chem.* **2010**, *20*, 1858–1867.
39. Hong, Y.; Häussler, M.; Lam, J.; Li, Z.; Sin, K.; Dong, Y.; Tong, H.; Liu, J.; Qin, A.; Renneberg, R.; *et al.* Label-Free Fluorescent Probing of G-Quadruplex Formation and Real-Time Monitoring of DNA Folding by a Quaternized Tetraphenylethene Salt with Aggregation-Induced Emission Characteristics. *Chem.—Eur. J.* **2008**, *14*, 6428–6437.
40. Tong, H.; Hong, Y.; Dong, Y.; Häussler, M.; Li, Z.; Lam, J. W. Y.; Dong, Y.; Sung, H. H.-Y.; Williams, I. D.; Tang, B. Z. Protein Detection and Quantitation by Tetraphenylethene-Based Fluorescent Probes with Aggregation-Induced Emission Characteristics. *J. Phys. Chem. B* **2007**, *111*, 11817–11823.
41. Wang, M.; Gu, X.; Zhang, G.; Zhang, D.; Zhu, D. Convenient and Continuous Fluorometric Assay Method for Acetylcholinesterase and Inhibitor Screening Based on the Aggregation-Induced Emission. *Anal. Chem.* **2009**, *81*, 4444–4449.
42. Guo, D.-S.; Liu, Y. Calixarene-Based Supramolecular Polymerization in Solution. *Chem. Soc. Rev.* **2012**, *41*, 5907–5921.
43. Wang, K.; Guo, D.-S.; Liu, Y. Temperature-Controlled Supramolecular Vesicles Modulated by *p*-Sulfonatocalix[5]arene with Pyrene. *Chem.—Eur. J.* **2010**, *16*, 8006–8011.
44. Wang, K.; Guo, D.-S.; Wang, X.; Liu, Y. Multistimuli Responsive Supramolecular Vesicles Based on the Recognition of *p*-Sulfonatocalixarene and Its Controllable Release of Doxorubicin. *ACS Nano* **2011**, *5*, 2880–2994.
45. Guo, D.-S.; Jiang, B.-P.; Wang, X.; Liu, Y. Calixarene-Induced Aggregation of Perylene Bisimides. *Org. Biomol. Chem.* **2012**, *10*, 720–723.
46. Guo, D.-S.; Chen, K.; Zhang, H.-Q.; Liu, Y. Nano-Supramolecular Assemblies Constructed from Water-Soluble Bis-(calix[5]arenes) with Porphyrins and Their Photoinduced Electron Transfer Properties. *Chem.—Asian J.* **2009**, *4*, 436–445.
47. Wang, K.; Guo, D.-S.; Liu, Y. Controlled Self-Assembly by Mono-*p*-sulfonatocalix[*n*]arenes and Bis-*p*-sulfonatocalix-[*n*]arenes. *Chem.—Eur. J.* **2012**, *18*, 8758–8764.
48. Guo, D.-S.; Wang, K.; Wang, Y.-X.; Liu, Y. Cholinesterase-Responsive Supramolecular Vesicle. *J. Am. Chem. Soc.* **2012**, *134*, 10244–10250.
49. Francisco, V.; Basilio, N.; Garcia-Rio, L.; Leis, J. R.; Maques, E. F.; Vázquez-Vázquez, C. Novel Catanionic Vesicles from Calixarene and Single-Chain Surfactant. *Chem. Commun.* **2010**, *46*, 6551–6553.
50. Moschetto, G.; Lauceri, R.; Gulino, F. G.; Sciotto, D.; Purrello, R. Non-covalent Synthesis in Aqueous Solution of Discrete Multi-porphyrin Aggregates with Programmable Stoichiometry and Sequence. *J. Am. Chem. Soc.* **2002**, *124*, 14536–14537.
51. Costanzo, L. D.; Geremia, S.; Randaccio, L.; Purrello, R.; Lauceri, R.; Sciotto, D.; Gulino, F. G.; Pavone, V. Calixarene-Porphyrin Supramolecular Complexes: pH-Tuning of the Complex Stoichiometry. *Angew. Chem., Int. Ed.* **2001**, *40*, 4245–4247.
52. Lau, V.; Heyne, B. Calix[4]arene Sulfonate as a Template for Forming Fluorescent Thiazole Orange H-Aggregates. *Chem. Commun.* **2010**, *46*, 3595–3597.
53. Basilio, N.; Gómez, B.; García-Río, L.; Francisco, V. Using Calixarenes To Model Polyelectrolyte Surfactant Nucleation Sites. *Chem.—Eur. J.* **2013**, *19*, 4570–4576.
54. Basilio, N.; Francisco, V.; Garcia-Rio, L. Aggregation of *p*-Sulfonatocalixarene-Based Amphiphiles and Supramphiphiles. *Int. J. Mol. Sci.* **2013**, *14*, 3140–3157.
55. Basilio, N.; García-Río, L. Sulfonated Calix[6]arene Host–Guest Complexes Induce Surfactant Self-Assembly. *Chem.—Eur. J.* **2009**, *15*, 9315–9319.
56. Basilio, N.; Martín-Pastor, M.; García-Río, L. Insights into the Structure of the Supramolecular Amphiphile Formed by a Sulfonated Calix[6]arene and Alkyltrimethylammonium Surfactants. *Langmuir* **2012**, *28*, 6561–6568.
57. Liu, J.; Jiang, N.; Ma, J.; Du, X. Insight into Unusual Downfield NMR Shifts in the Inclusion Complex of Acridine Orange with Cucurbit[7]uril. *Eur. J. Org. Chem.* **2009**, 4931–4938.
58. Biedermann, F.; Elmalem, E.; Ghosh, I.; Nau, W. M.; Scherman, O. A. Strongly Fluorescent, Switchable Perylene Bis(diimide) Host–Guest Complexes with Cucurbit[8]uril in Water. *Angew. Chem., Int. Ed.* **2012**, *51*, 7739–7743.
59. Dsouza, R. N.; Pischel, U.; Nau, W. M. Fluorescent Dyes and Their Supramolecular Host–Guest Complexes with Macrocycles in Aqueous Solution. *Chem. Rev.* **2011**, *111*, 7941–7980.
60. Uchiyama, S.; Kawai, N.; de Silva, A. P.; Iwai, K. Fluorescent Polymeric AND Logic Gate with Temperature and pH as Inputs. *J. Am. Chem. Soc.* **2004**, *126*, 3032–3033.
61. Li, C.; Liu, S. Polymeric Assemblies and Nanoparticles with Stimuli-Responsive Fluorescence Emission Characteristics. *Chem. Commun.* **2012**, *48*, 3262–3278.
62. Qu, D.-H.; Wang, Q.-C.; Ma, X.; Tian, H. A [3]Rotaxane with Three Stable States That Responds to Multiple-Inputs and Displays Dual Fluorescence Addresses. *Chem.—Eur. J.* **2005**, *11*, 5929–5937.
63. Dube, H.; Ams, M. R.; Rebek, J., Jr. Supramolecular Control of Fluorescence through Reversible Encapsulation. *J. Am. Chem. Soc.* **2010**, *132*, 9984–9985.
64. Raymo, F. M.; Tomasulo, M. Electron and Energy Transfer Modulation with Photochromic Switches. *Chem. Soc. Rev.* **2005**, *34*, 327–336.
65. Tian, H.; Yang, S. J. Recent Progresses on Diarylethene Based Photochromic Switches. *Chem. Soc. Rev.* **2004**, *33*, 85–97.
66. Irie, M.; Fukaminato, T.; Sasaki, T.; Tamai, N.; Kawai, T. Organic Chemistry: A Digital Fluorescent Molecular Photoswitch. *Nature* **2002**, *420*, 759–760.
67. Chung, J. W.; Yoon, S.-J.; Lim, S.-J.; An, B.-K.; Park, S. Y. Dual-Mode Switching in Highly Fluorescent Organogels: Binary Logic Gates with Optical/Thermal Inputs. *Angew. Chem., Int. Ed.* **2009**, *48*, 7030–7034.
68. Jiang, G.; Wang, S.; Yuan, W.; Zhao, Z.; Duan, A.; Xu, C.; Jiang, L.; Song, Y.; Zhu, D. Photo- and Proton-Dual-Responsive Fluorescence Switch Based on a Bisthienylethene-Bridged Naphthalimide Dimer and Its Application in Security Data Storage. *Eur. J. Org. Chem.* **2007**, 2064–2067.
69. Schultz, A.; Laschat, S.; Diele, S.; Nimtz, M. Tetraphenylethene-Derived Columnar Liquid Crystals and Their Oxidative Photocyclization. *Eur. J. Org. Chem.* **2003**, 2829–2839.
70. Aldred, P.; Li, C.; Zhu, M.-Q. Optical Properties and Photooxidation of Tetraphenylethene-Based Fluorophores. *Chem.—Eur. J.* **2012**, *18*, 16037–16045.
71. Huang, G.; Ma, B.; Chen, J.; Peng, Q.; Zhang, G.; Fan, Q.; Zhang, D. Dendron-Containing Tetraphenylethylene

Compounds: Dependence of Fluorescence and Photocyclization Reactivity on the Dendron Generation. *Chem.—Eur. J.* **2012**, *18*, 3886–3892.
72. Guo, D.-S.; Wang, K.; Liu, Y. Selective Binding Behaviors of *p*-Sulfonatocalixarenes in Aqueous Solution. *J. Incl. Phenom. Macrocycl. Chem.* **2008**, *62*, 1–21.
73. Tong, H.; Hong, Y.; Dong, Y.; Häußler, M.; Lam, J. W. Y.; Li, Z.; Guo, Z.; Guo, Z.; Tang, B. Z. Fluorescent "Light-Up" Bioprobes Based on Tetraphenylethylene Derivatives with Aggregation-Induced Emission Characteristics. *Chem. Commun.* **2006**, 3705–3707.
74. Wang, J.; Mei, J.; Hu, R.; Sun, J. Z.; Qin, A.; Tang, B. Z. Click Synthesis, Aggregation-Induced Emission, *E*/*Z* Isomerization, Self-Organization, and Multiple Chromisms of Pure Stereoisomers of a Tetraphenylethene-Cored Luminogen. *J. Am. Chem. Soc.* **2012**, *134*, 9956–9966.
75. Yu, W.-H.; Chen, C.; Hu, P.; Wang, B.-Q.; Redshaw, C.; Zhao, K.-Q. Tetraphenylethene-Triphenylene Oligomers with an Aggregation-Induced Emission Effect and Discotic Columnar Mesophase. *RSC Adv.* **2013**, *3*, 14099–14105.
76. Watanabe, S.; Kobayashi, A.; Kakimoto, M.; Imai, Y. Synthesis and Characterization of New Aromatic Polyesters and Polyethers Derived from 1,2-Bis(4-hydroxyphenyl)-1,2-diphenylethylene. *J. Polym. Sci., Part A: Polym. Chem.* **1994**, *32*, 909–915.
77. Arena, G.; Contino, A.; Lombardo, G. G.; Sciotto, D. Water-Soluble Calix[6]arenes. Characterization of 5,11,17,23,29,35-Hexasulphonate-37,38,39,40,41,42-hexahydroxy-calix[6]-arene and Thermodynamic Study of Proton Complex Formation. *Thermochim. Acta* **1995**, *264*, 1–11.
78. Guo, D.-S.; Chen, S.; Qian, H.; Zhang, H.-Q.; Liu, Y. Electrochemical Stimulus-Responsive Supramolecular Polymer Based on Sulfonatocalixarene and Viologen Dimers. *Chem. Commun.* **2010**, *46*, 2620–2622.
79. Xu, X.; Lv, W.; Huang, J.; Li, J.; Tang, R.; Yan, J.; Yang, Q.; Qin, J.; Li, Z. Functionalization of Graphene by Tetraphenylethylene Using Nitrene Chemistry. *RSC Adv.* **2012**, *2*, 7042–7047.
80. Gu, Z.-Y.; Guo, D.-S.; Sun, M.; Liu, Y. Effective Enlargement of Fluorescence Resonance Energy Transfer of Polyporphyrin Mediated by $\beta$-Cyclodextrin Dimers. *J. Org. Chem.* **2010**, *75*, 3600–3607.